Supplementary information
Nickel–Iron–Cobalt (Hydr)oxide-Decorated Carbon Nanotube Forest for the Oxygen-Evolution Reaction

Mahdieh Maleki,[a] Lilla Nánai,[b] Sergey K. Zharmukhamedov,[c] Robabeh Bagheri,[a] Nader Akbari,[d] Elena V. Zadneprovskaya,[e] Roman A. Voloshin,[e] Klara Hernadi,[b*] Suleyman I. Allakhverdiev,[e,f*] and Mohammad Mahdi Najafpour[d,e*]

[a]Department of Chemistry, Institute for Advanced Studies in Basic Sciences (IASBS), 45137-66731, Zanjan, Iran
[b]Institute of Physical Metallurgy, Metal Forming and Nanotechnology, University of Miskolc, 3515 Miskolc-Egyetemváros, C/2-5 Building 209, Hungary
[c]Institute of Basic Biological Problems, FRC PSCBR RAS, Moscow Region, 142290, Pushchino, Russia
[d]Department of Chemistry, Sharif University of Technology, Tehran, 11155−9516, Iran
[e]K. A. Timiryazev Institute of Plant Physiology RAS, Botanicheskaya Street 35, Moscow, 127276, Russia
[f]Faculty of Engineering and Natural Sciences, Bahçeşehir University, Istanbul, Turkey
*E-mails: klara.hernadi@uni-miskolc.hu (KH); suleyman.allakhverdiev@gmail.com (SA); mmnajafpour@sharif.edu (MMN).

Table of contents

Experimental Section

Materials

Nickel(II) nitrate hexahydrate ($Ni(NO_3)_2 \cdot 6H_2O$, >99% trace metals basis), cobalt(II) chloride hexahydrate ($CoCl_2 \cdot 6H_2O$, ≥98.0%), and iron(III) nitrate nonahydrate ($Fe(NO_3)_3 \cdot 9H_2O$, >99% trace metals basis) were purchased from Sigma-Aldrich and used as received. Other chemicals, including reagents and solvents, were obtained from commercial vendors. Unless otherwise stated, these materials were used directly as received and were not subjected to any additional purification steps. For all solution preparation and experimental procedures requiring water, ultrapure Milli-Q water was employed. The resistivity of the Milli-Q water was maintained in the range of 18 MΩ·cm (measured at 25 °C), and this water quality was used consistently across all experiments to ensure reproducibility and to minimize the influence of ionic impurities.

Characterization

Phase identification and crystallographic characterization of the prepared samples were conducted using powder X-ray diffraction (XRD). XRD patterns were collected on a Bruker D8 Advance diffractometer (Germany) equipped with a Cu Kα radiation source. The resulting diffraction patterns were used to evaluate the structural features and assess the presence of crystalline phases. Elemental analysis and compositional quantification were performed using inductively coupled plasma–optical emission spectroscopy (ICP–OES). Measurements were acquired on a Varian 730-ES instrument, providing quantitative information on elemental content as part of the overall characterization workflow. The surface morphology and microstructural features of the materials were examined by scanning electron

microscopy (SEM). SEM images were obtained using a MIRA 3 TESCAN system, enabling visualization of particle shape, surface texture, and morphological uniformity at the microscale. The experiments focusing on the oxygen-evolution reaction were carried out using an HQ40d portable dissolved oxygen meter.

Electrochemical Characterization

Electrochemical measurements were carried out using an EmStat3+ potentiostat (PalmSens, Netherlands). All experiments were performed in a polystyrene electrochemical cell. Cyclic voltammetry (CV) was conducted using a conventional three-electrode configuration to ensure reliable potential control and separation of working and counter-electrode processes. In this setup, CNT F served as the working electrode, Hg/HgO was used as the reference electrode for all OER experiments, and a platinum foil electrode functioned as the counter electrode. Unless otherwise noted, all electrochemical potentials in this work are referenced to the reversible hydrogen electrode (RHE). The 1.0 M KOH electrolyte used for OER testing was prepared from commercially available reagents and was neither CO_2-free nor further purified. No O_2 bubbling or gas purging was employed during the electrochemical measurements; all tests were conducted in a stationary, unstirred cell. During electrochemical testing, the temperature of the experimental environment was monitored using a Laserliner 082 thermometer (Germany) to track potential temperature-related variations in electrochemical response and to support consistency between measurements.

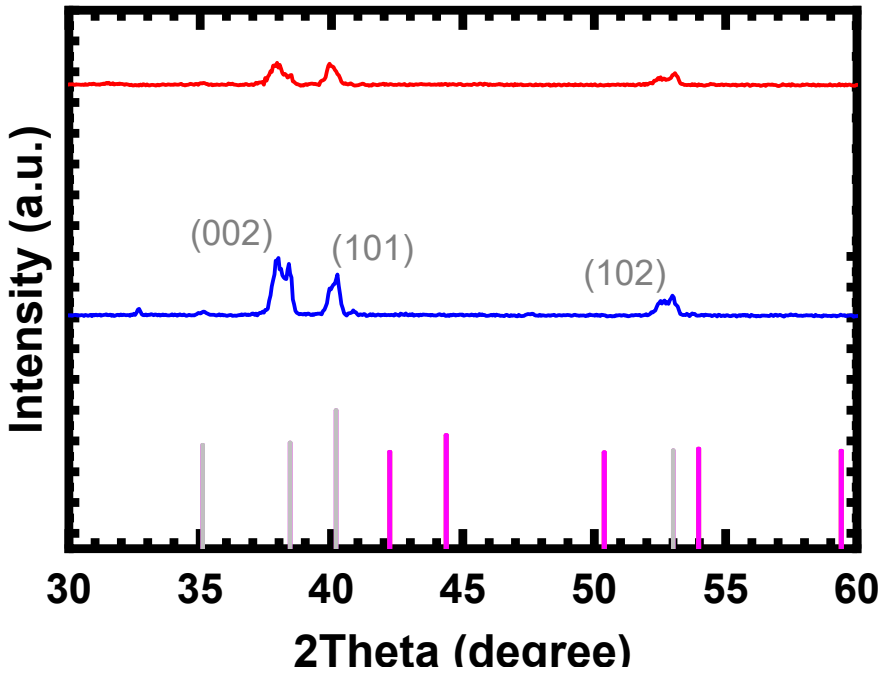

Figure S1 XRD patterns of F1 collected before (blue) and after (red) OER. Metallic Ti (Ref. Code:00-044-1294) and graphite (Ref. Code: 00-056-0159) patterns are shown in grey and pink, respectively.

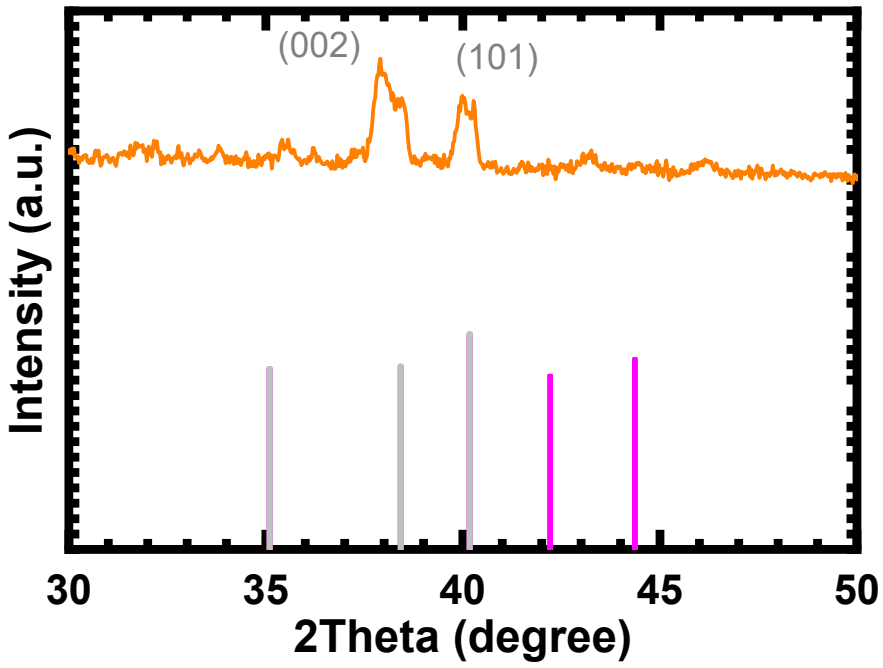

Figure S2 XRD pattern of F2. In addition to Ti reflections, broad humps at ≈43° and ≈46° (2θ, Cu Kα) indicate a poorly crystalline/nanocrystalline NiFeCo (hydr)oxide deposit rather than sharp crystalline metal peaks. Metallic Ti (Ref. Code: Reference code:00-044-1294) and graphite (Ref. Code: 00-056-0159) patterns are shown in grey and pink, respectively.

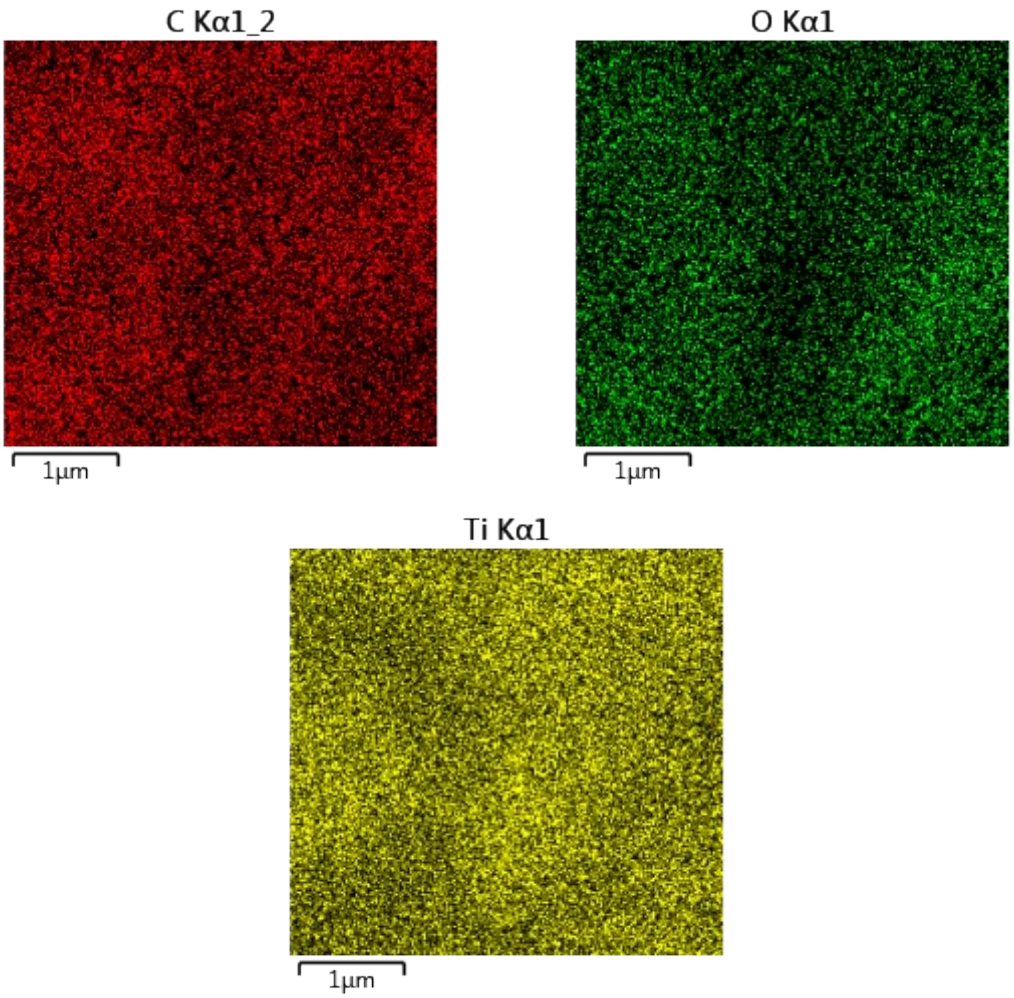

Figure S3 SEM–EDS elemental maps of the CNT forest (CNT F), showing the distribution of C, Ti, and O, before metal oxide loading.

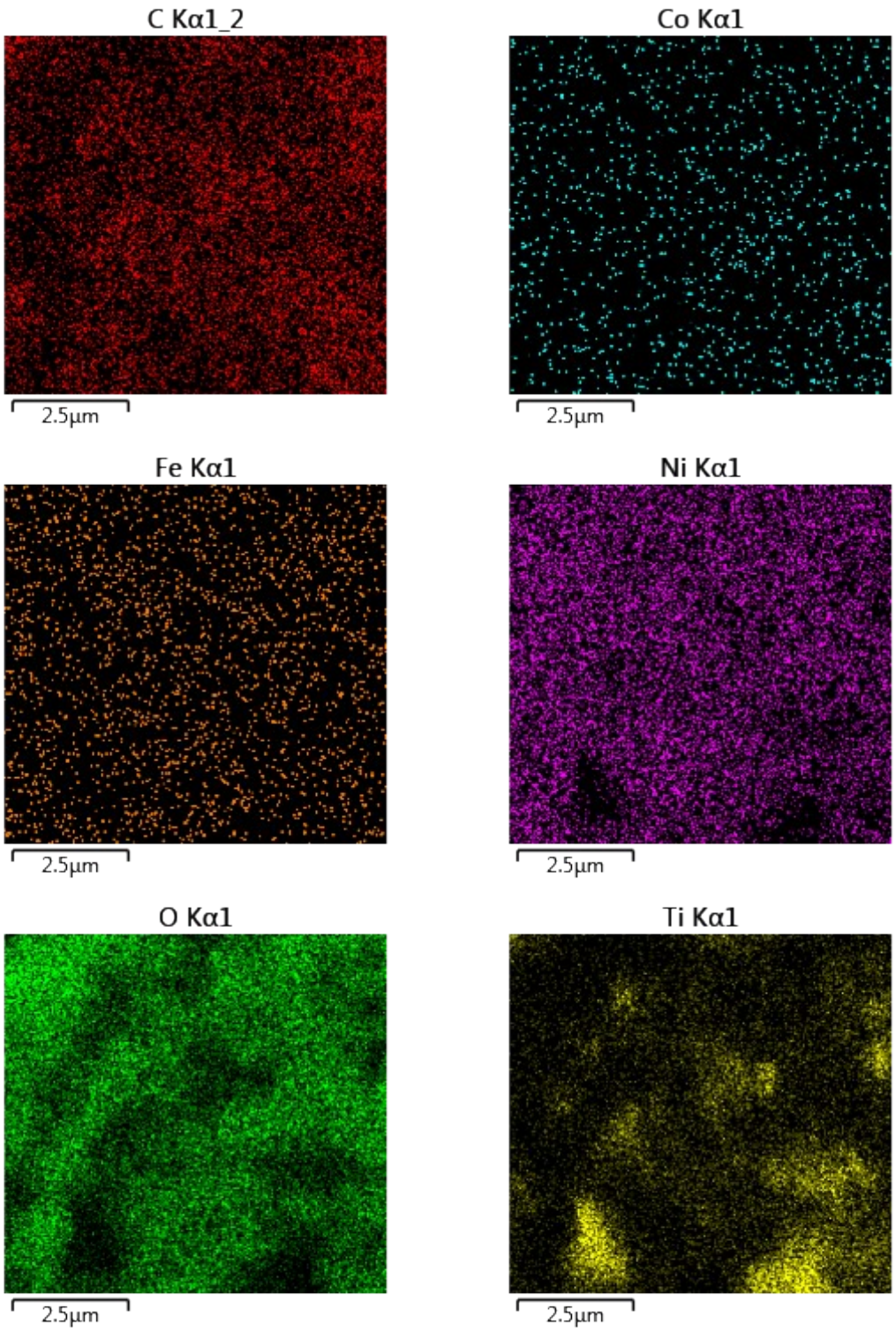

Figure S4 SEM–EDS elemental maps of F1 before OER, highlighting Ni incorporation in the CNT forest together with C (support) and O (oxide/(hydr)oxide-related signal).

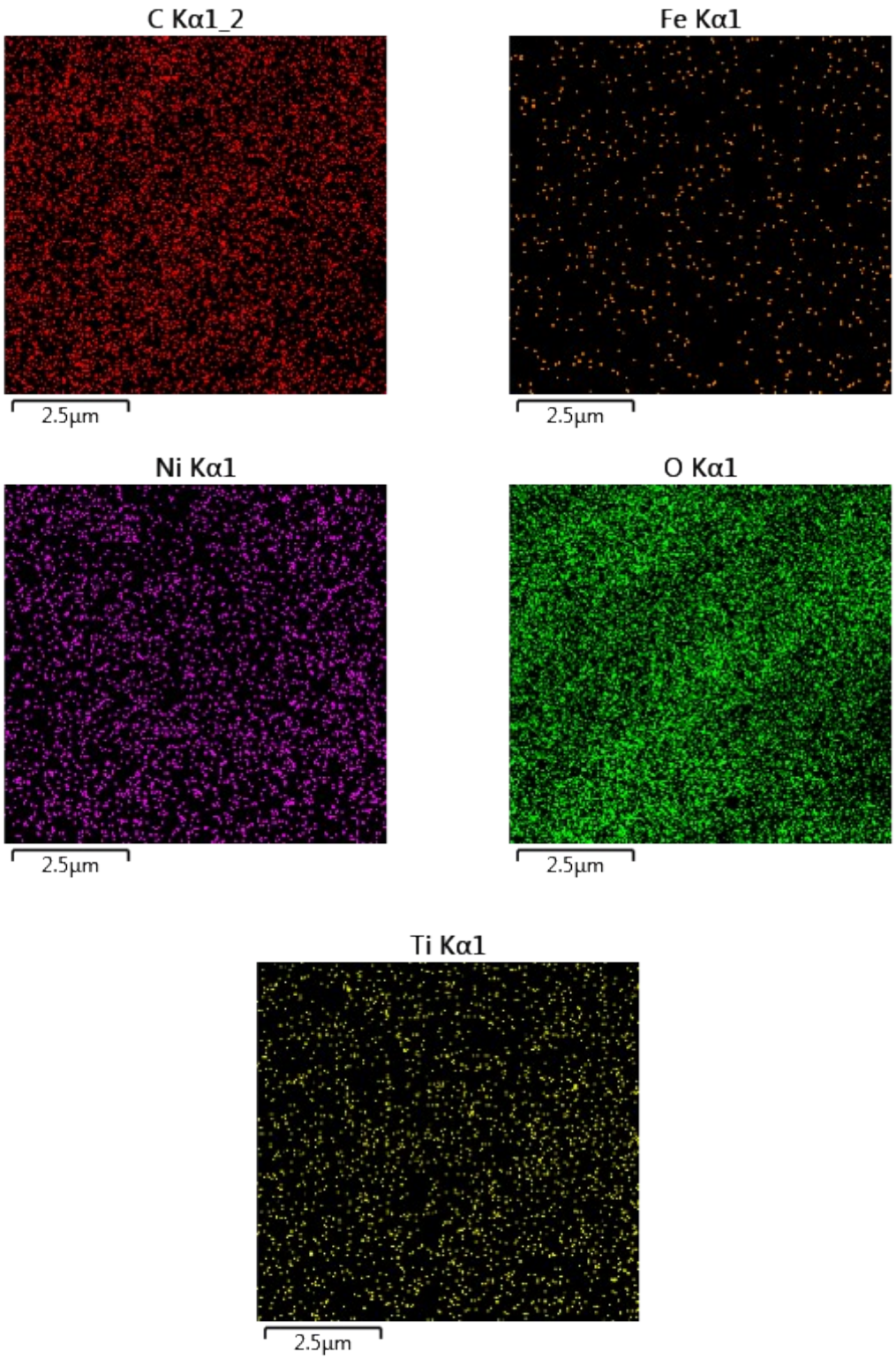

Figure S5 SEM–EDS elemental maps of F1 after OER, showing the elemental distribution of Ni, O, C, Fe, and Ti following anodic testing. The maps highlight Ni/O-rich regions and structural degradation of the carbon scaffold.

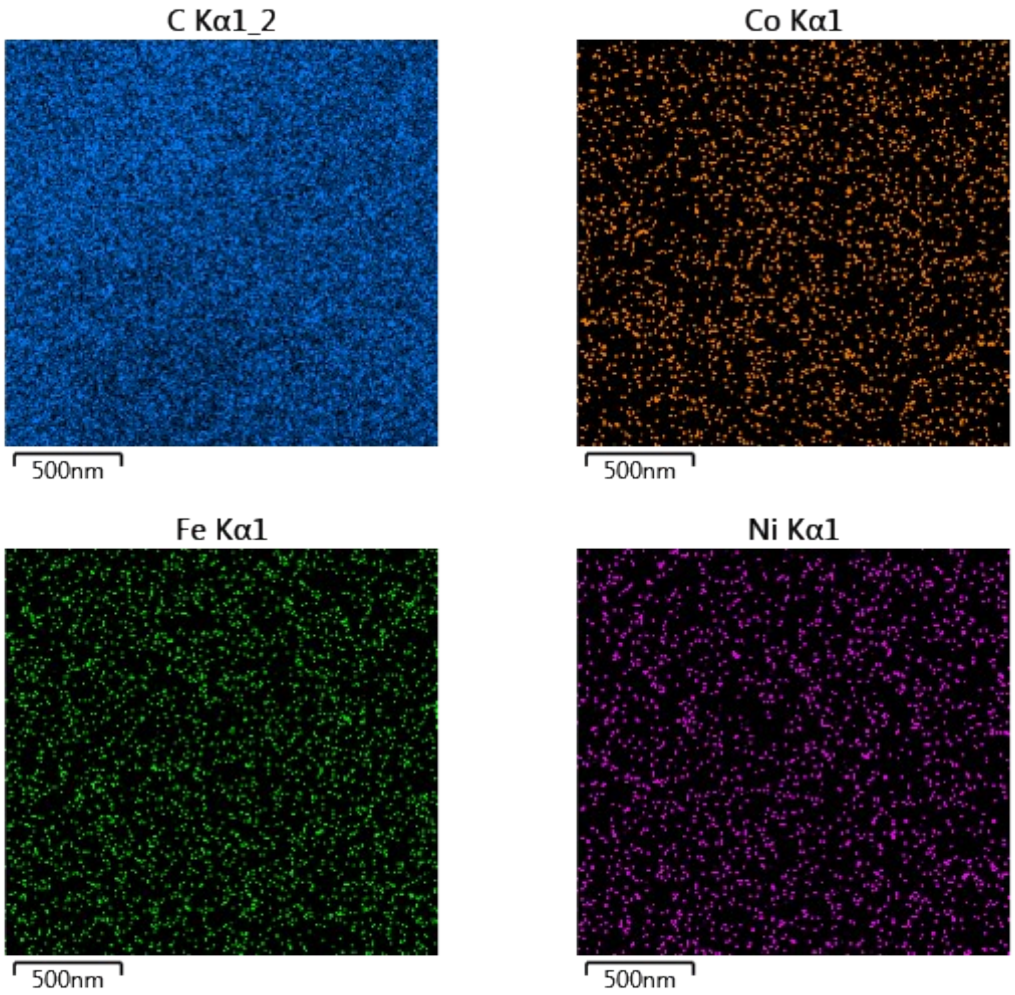

Figure S6 SEM–EDS elemental maps of F2, confirming the simultaneous presence and surface dispersion.

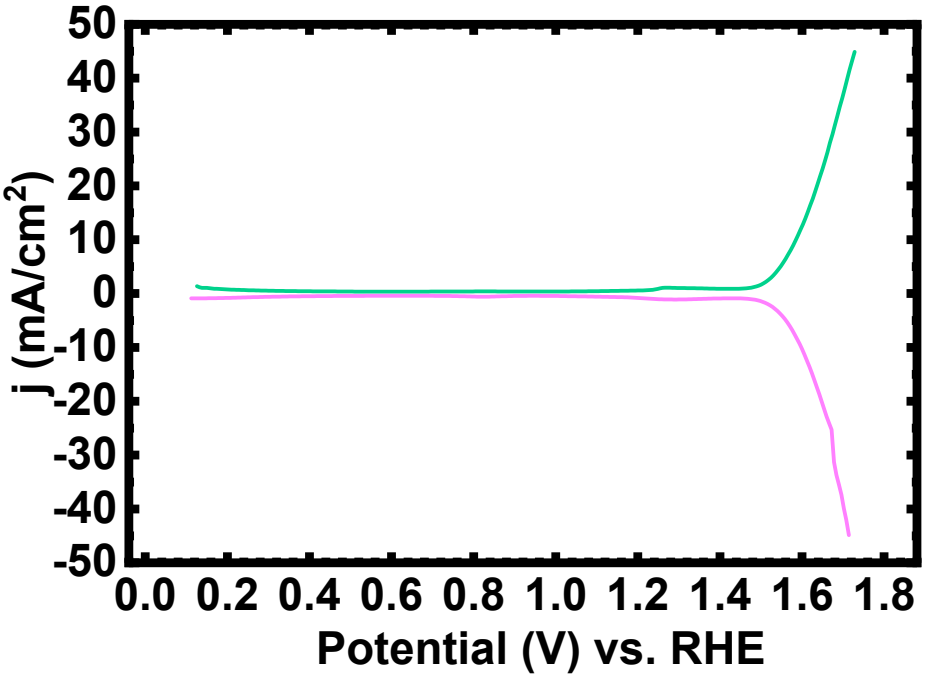

Figure S7 Square-wave voltammetry (SWV) of F2 in alkaline electrolyte (amplitude: 1.0 V; frequency: 1 Hz).

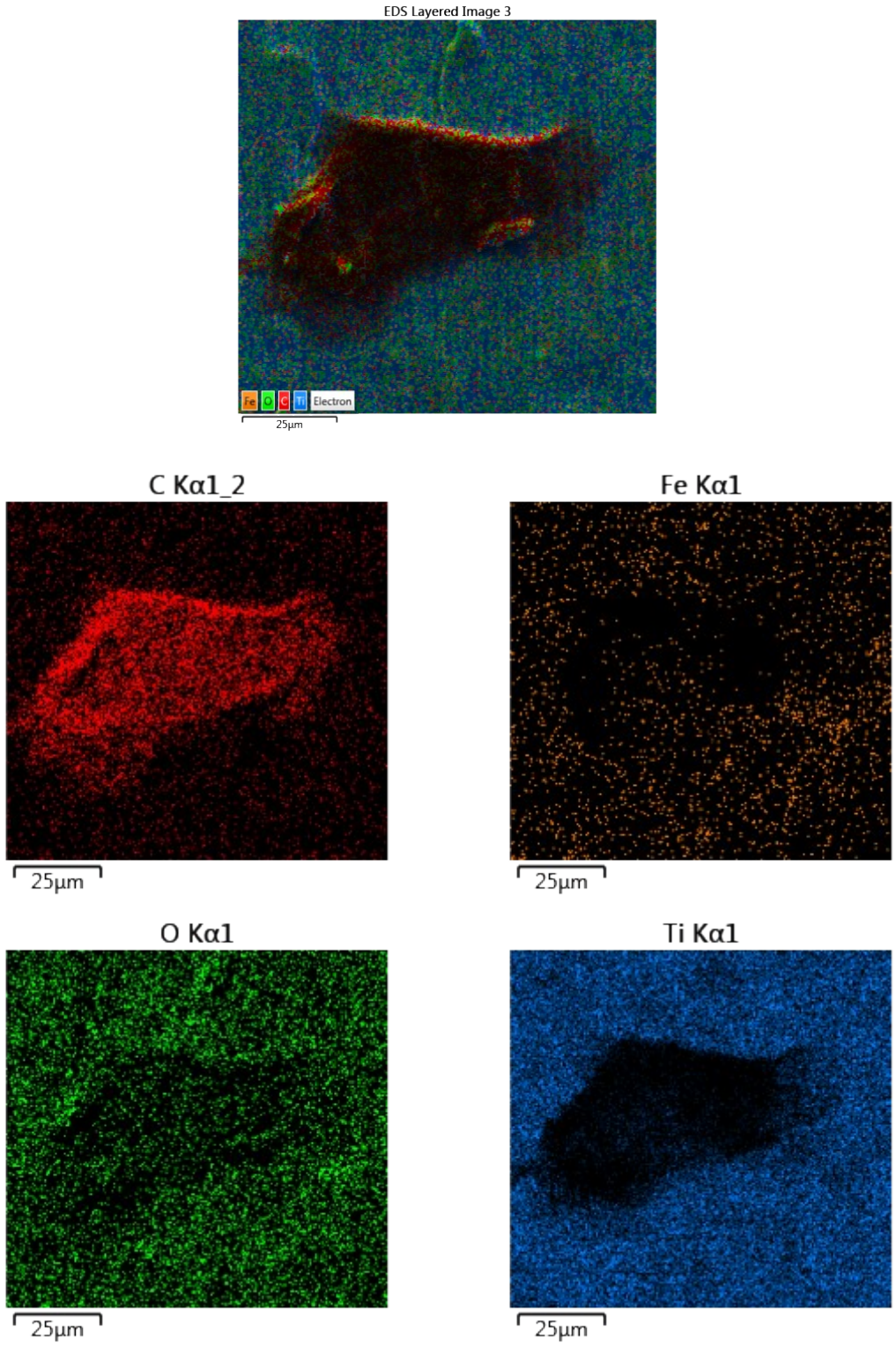

Figure S8 SEM–EDS elemental maps of F2 after 20 hours at 1.55 V. Only small areas containing carbon were observed.

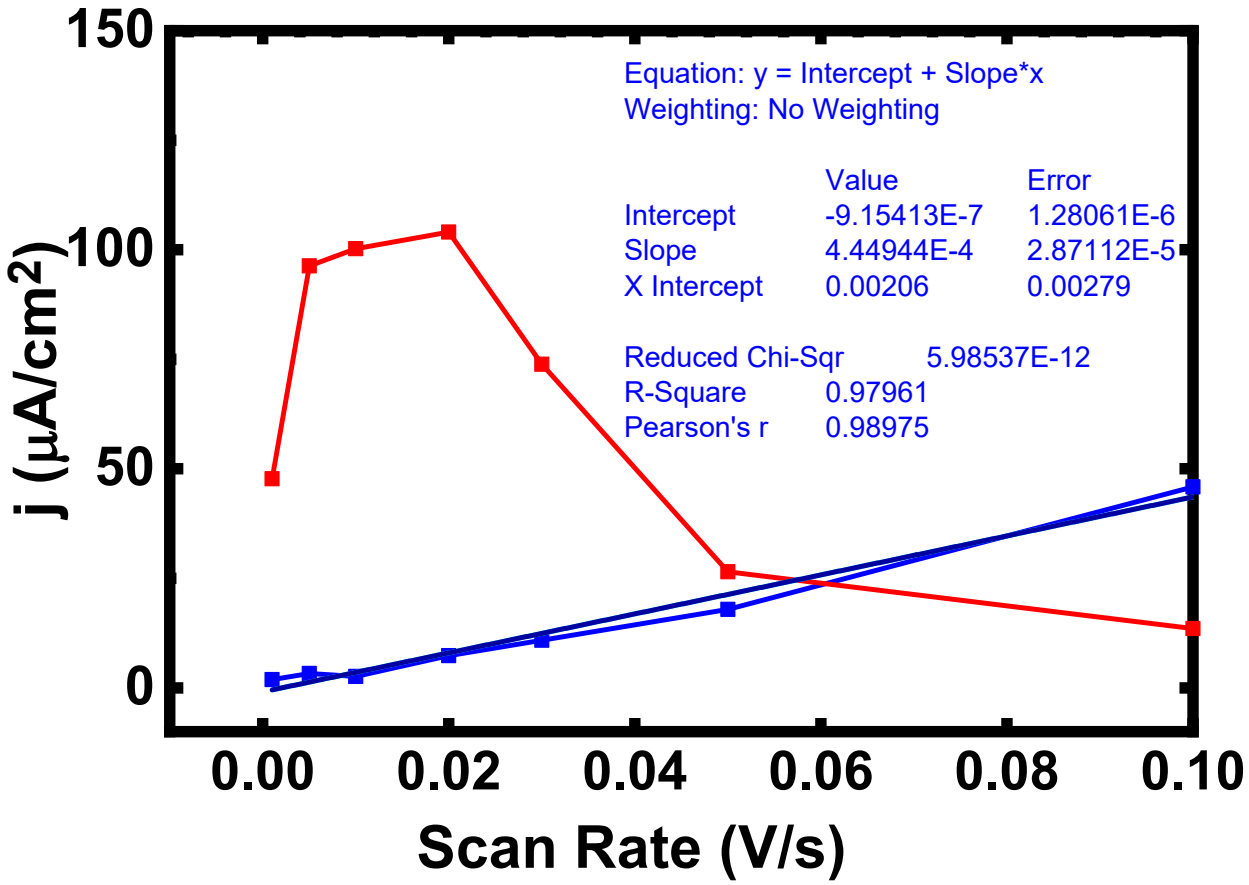

Figure S9 Current density (j) as a function of scan rate for CNT F (blue) and F2 (red).

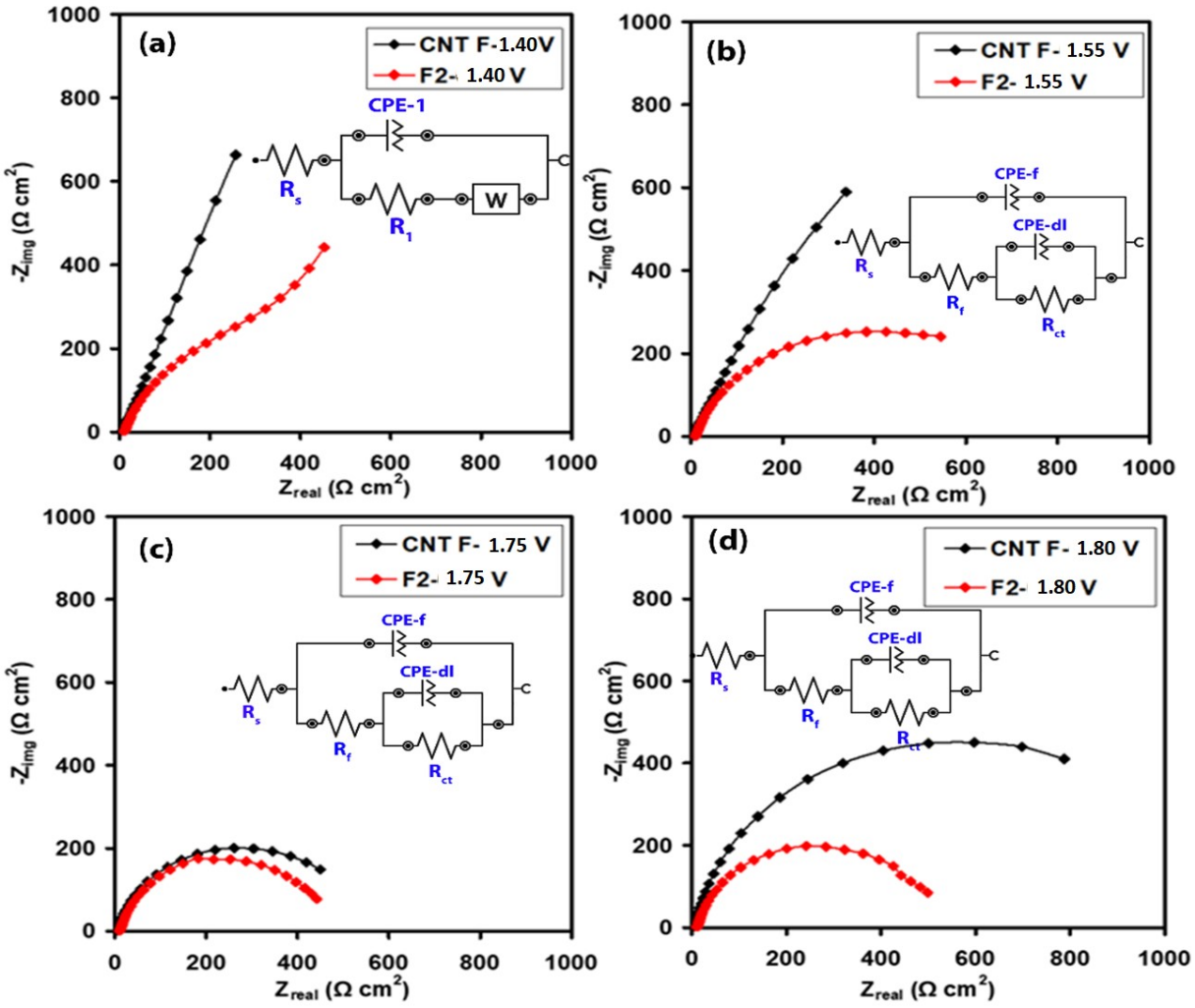

Figure S10 Nyquist plots for the CNT F and F2 catalysts at various applied potentials: 1.40 V (a), 1.55 V (b), 1.75 V (c) and 1.80 V (d) fitted using equivalent circuits presented as inset.

Table S1 Electrochemical impedance parameters for the CNT F and F2 catalyst at various applied potentials, fitted using equivalent circuits presented as inset.

Sample	Potential (V)	Rs (Ω cm^2)	CPE		R_f (Ω cm^2)	W			CPE		R_{ct} (Ω cm^2)
			$Q\times10^{-5}$ (Ω^{-1} $cm^{-2}S^n$)	n		T	P	n	$Q\times10^{-5}$ (Ω^{-1} $cm^{-2}S^n$)	n	
CNT F	1.40	6.77	1.98	0.95	50.4	5212	0.32	0.70	-	-	-
	1.55	6.79	1.82	0.95	48.0	-	-	-	9.32	0.69	4599
	1.75	6.92	1.11	0.99	30.9	-	-	-	3.86	0.74	483
	1.80	6.90	1.07	0.99	49.1	-	-	-	1.62	0.81	980
F2	1.40	10.55	3.61	0.81	590.2	4054	0.51	0.76	-	-	-
	1.55	10.61	3.12	0.82	448.2	-	-	-	74.7	0.34	645
	1.75	10.77	2.17	0.85	104.3	-	-	-	0.11	0.99	350
	1.90	10.93	1.79	0.86	96.34	-	-	-	0.10	0.99	406